ISSN 1062-8738, Bulletin of the Russian Academy of Sciences: Physics, 2022, Vol. 86, No. 3, pp. 249–255. © Allerton Press, Inc., 2022.
Russian Text © The Author(s), 2022, published in Izvestiya Rossiiskoi Akademii Nauk, Seriya Fizicheskaya, 2022, Vol. 86, No. 3, pp. 322–328.

Spatial Features of a Super Substorm in the Main Phase of the Magnetic Storm of April 5, 2010

I. V. Despirak[a], *, N. G. Kleimenova[b], L. I. Gromova[c], A. A. Lubchich[a], V. Guineva[d], and P. V. Setsko[a]

[a] *Polar Geophysical Institute, Apatity, 184209 Russia*

[b] *Schmidt Institute of Physics of the Earth, Moscow, 123995 Russia*

[c] *Pushkov Institute of Terrestrial Magnetism, Ionosphere and Radio Wave Propagation, Moscow, 108840 Russia*

[d] *Space Research and Technology Institute, Bulgarian Academy of Sciences, Stara Zagora, 6000 Bulgaria*

**e-mail: despirak@gmail.com*

Received October 15, 2021; revised November 5, 2021; accepted November 22, 2021

Abstract—The spatial distribution of electrojets during a super substorm on April 5, 2010, is investigated using magnetic data from AMPERE satellite mission and the global SuperMAG, INTERMAGNET, and IMAGE networks. The super substorm was observed during the main phase of a moderate magnetic storm (*Dst* ~ −81 nT). It is shown that an unusually strong westward night electrojet developed on a global scale, from the evening sector to the day sector through midnight. An intense eastward electrojet in the evening sector is detected, due possibly to the formation of an additional partial ring current during the super substorm. The complex latitudinal layered structure of the electrojets is observed on the day side.

DOI: 10.3103/S106287382203008X

INTRODUCTION

Super substorms (SSSes) began to be studied relatively recently. This term originally meant intense substorms observed on the SuperMAG magnetometer networks with ultrahigh values of the *SML* index of geomagnetic activity (<−2500 nT) [1]. Despite the brief period of studying these intense events, different aspects of them have been examined: the dependence of SSS emergence on solar activity [2], the presence and intensity of magnetic storms [1, 2], and the large-scale structure of the solar wind [3]. It was shown that SSSes develop only during coronal mass ejections (CMEs), specifically during interplanetary magnetic clouds (IMCs), at the front of compressed plasma (sheath) before a magnetic cloud at high negative values of IMF B_Z component, and upon local jumps in the density and dynamic pressure of the solar wind [4]. The correlation between SSSes and the *PC* index of the polar cap, field aligned currents (FACs), interplanetary electric and magnetic fields [5, 6], and geomagnetic induced currents (GICs) has also been studied [7].

However, aspects of the development of auroral disturbances (auroras and electrojets) have been studied little during super substorms. There are only several works on this subject that consider separate SSS events. It was found that auroras developed in an unusual manner during SSSes. For example, there is no standard increase in brightness of the equatorial arc itself before a super substorm. No increase is observed in the night sector before an aurora's breakup and subsequent jump poleward [8]. In addition, the western electrojet extends considerably in azimuth [9, 10].

This paper considers the interesting case of a super substorm in which a western and eastern electroject developed in an unusual manner. The SSS event was observed on April 5, 2010 during the development of the first magnetic storm (*Dst* ~ −81 nT) of solar cycle 24. Many works have been dedicated to studying this storm [8, 11–16]. Results of the SSS study were reviewed in [16]. It was shown that in contrast to normal substorms, an intense eastern ionospheric current related to intensification of the partial ring current often appears in the day sector during a super substorm.

The aim of this paper is to analyze the spatial distribution of geomagnetic disturbances during the super substorm of April 5, 2010, using data from AMPERE satellite mission and the global SuperMAG, INTERMAGNET, and IMAGE networks of magnetometers, and to interpret the results based on concepts of global current systems. We analyze disturbances at both polar and auroral latitudes, and midlatitude positive bays usually associated with the development of the substorm current wedge [17].

EXPERIMENTAL DATA

This work is based on an analysis of observations from SuperMAG (http://supermag.jhuapl.edu/) [18] and INTERMAGNET (https://www.intermag-

net.org/) [19] ground-based magnetometers, and the Scandinavian meridional IMAGE profiles (http://space.fmi.fi/image/) [20]. The global spatial distribution of electrojets was determined from maps of magnetic field vectors obtained on the SuperMAG network, and maps from a spherical harmonic analysis of the distribution of magnetic vectors in the ionosphere and field-aligned currents obtained using data from the low-apogee *Iridium* communication satellites of the AMPERE system (Active Magnetosphere and Planetary Electrodynamics Response Experiment, http://ampere.jhuapl.edu). The AMPERE project includes simultaneous recording of the magnetic field by 66 satellites, and maps being constructed every 2 min with averaging over 10 min [21].

The conditions in the solar wind and the interplanetary magnetic field (IMF) before the onset of an SSS were determined using the OMNI CDAWeb database (http://cdaweb.gsfc.nasa.gov/). The streams and structures of the solar wind were determined using a catalog of large-scale solar wind phenomena (ftp://ftp.iki.rssi.ru/omni/) [22].

INTERPLANETARY CONDITIONS DURING THE MAGNETIC STORM OF APRIL 5, 2010

The storm of April 5, 2010, was caused by a large interplanetary coronal mass ejection (ICME) arriving at the Earth. Its source was a B7.4 class solar flare recorded at 09:04 UT on April 3, 2010. According to estimates [23], the initial velocity of the ICME in the vicinity of the sun was around 1100 km/s, while the velocity of the leading edge of ICME at the Earth's orbit was nearly 800 km/s.

The coronal mass ejection reached the Earth's orbit on April 5, 2010, around 08:26 UT [16] and caused a moderate but prolonged magnetic storm ($Dst \sim -81$ nT). Figure 1 presents data on the parameters of the solar wind and the interplanetary magnetic field (IMF) over the period from 06:00 UT on April 5 to 18:00 UT on April 6, 2010 (on the left), and from 06:00 to 16:00 UT on April 5, 2010 (on the right). The variations in the B_T value of the magnetic field, B_Y and B_Z components of the IMF, the velocity (V) and dynamic pressure (P_{dyn}) of the solar wind, and such geomagnetic indices as *PC*, *SYM/H*, and *SML* are shown from top to bottom. The magnetic cloud (MC) and the region of compressed plasma are indicated, and their boundaries are marked by solid and dashed red lines (on the left) and a horizontal arrow (on the right). The moment of maximum SSS development is shown by the vertical blue line.

The front of the coronal ejection (sheath) reached the Earth's orbit at 08:26 UT, with a magnetic cloud passing from ~13:00 UT on April 5 to ~15:00 UT on April 6. High negative values of up to −15 nT were observed for the IMF's B_Z component upon the arrival of the sheath region, which likely started the development of the long-lasting magnetic storm with the intensity of ~−81 nT. A super substorm (SSS) was recorded at the beginning of the storm ($Dst \sim -20$ nT) during the sheath, under increasing pressure, density, and B_T of the magnetic field. Inside the region of the sheath, the IMF B_Z component changed its sign several times and reached values of ~−15 nT.

The onset of the super substorm was recorded at ~08:26 UT, according to the sharp drop in the *SML* index (Fig. 1, right panel) and the X component of the magnetic field at the Alaska stations (FYU, CMO, and GAK) (Fig. 2). The expantion phase lasted for ~1 h until ~09:30 UT (when the *SML* index began to fall to the minimum), having intensified three times (~09:03, ~09:17, and ~09:29 UT). Once the *SML* index reached its lowest value (−2351 nT), the recovery phase began and continued until ~11:30 UT, when the *SML* index returned to the pre-super substorm level after several intensifications. The gradual development of the SSS observed during the growth and expantion phases was described in detail in [8, 15], where the development of auroras over Alaska was analyzed.

DEVELOPMENT OF MAGNETIC DISTURBANCES ON THE EVENING AND NIGHT SIDES

At the onset of the super substorm, the stations in the American sector were in the evening and midnight sectors. The maps of magnetic vectors from the SuperMAG network presented in Fig. 2a show the global spatial distribution of magnetic disturbances while indicating the positions of some terrestrial stations with magnetograms provided below in Figs. 2b, 2c, and 3. The maps are constructed for three local minima in the *SML* index (09:03, 09:17, and 09:29 UT) according to the jump-wise development of this super substorm. We can see the disturbances grew stronger with each new intensification, and the region of their occurrence expanded (from polar to middle latitudes). The highest intensity of disturbances was recorded in the evening and night sectors where the American sector stations were located. Figure 2a also shows that the westward electrojet was observed in a very broad longitudinal sector, from the evening (Alaska) to the morning (Greenland) and day sectors (Scandinavia).

Figures 2b, 2c present magnetograms from selected stations in the United States and Greenland. Figure 2b shows variations in the X component of the magnetic field from 06:00 to 13:00 UT on April 5, 2010, for the stations in Alaska (KAV, FYU, CMO, and GAK) located in the auroral zone (from ~63.4° to ~71.5° CGLAT). At 08:30 UT, strong magnetic field variations began that showed three minima (~2500 nT) corresponding to three intensifications. The lower panels in Fig. 2b show disturbances of the X component at

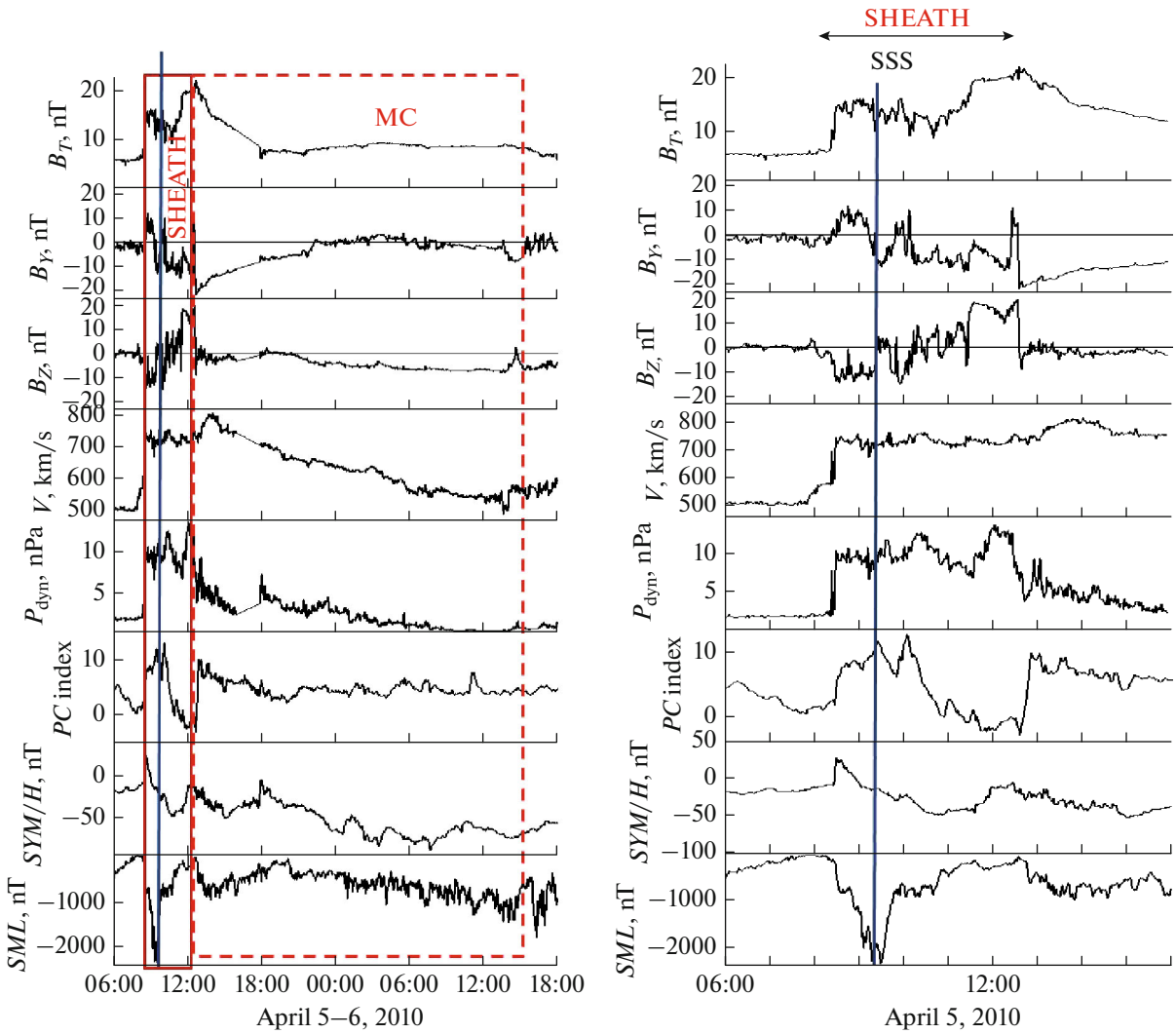

Fig. 1. Parameters of the solar wind and IMF plus *PC*, *SYM/H*, and *SML* geomagnetic indices for the intervals from 06:00 UT on April 5, 2010, to 18:00 UT on April 6 (left) and 06:00 to 16:00 UT on April 5 (right). From top to bottom: variations in the B_T value of the magnetic field; IMF components B_Y and B_Z in the GSM system; velocity and dynamic pressure of the solar wind; and *PC*, *SYM/H*, and *SML* geomagnetic indices. Boundaries of the magnetic cloud and the region of the compressed plasma sheath are marked by vertical solid and dashed red lines (left) and the horizontal blue line (right). The moments of SSS observation are shown by the vertical blue line.

stations FRN and HON in the same longitude sector at middle latitudes (42.6° and 20.1° CGLAT). Fairly intense positive bays (~60 and ~30 nT) were recorded here in a wide range of latitudes (~20° CGLAT).

Figure 2c shows variations in the *X* component for stations of the post-midnight (SMI, MEA) and morning sectors (NAQ) of the auroral zone (from ~65.8° to ~67.5° CGLAT) and the midlatitude stations (FRD, BOU, TUC) (from ~48.5° to ~39.3° CGLAT). We can see that in contrast to the night sector, the negative bays were less intense (~−1200 nT) in the morning sector and were observed at higher latitudes. Positive bays (~20–30 nT) were detected at midlatitude stations FRD, BOU, and TUC.

DEVELOPMENT OF MAGNETIC DISTURBANCES ON THE DAY SIDE

Figure 3 shows the magnetic disturbances from 04:00 to 12:00 UT on April 5, 2010, recorded by the IMAGE chain of magnetometers (from ~57.3° to ~76.6° CGLAT) and at several stations of middle and low latitudes, e.g., BOX, KIV, PAG, and TAM (from ~8.9° to ~54.5° CGLAT). Stations BJN–NAL recorded negative magnetic bays (~−700 nT) at polar latitudes (>~70° CGLAT). At auroral latitudes, the bays became positive (~+500 nT) at stations SOR–SOD (~67.8–63.9° CGLAT). Starting from station NUR (~57.3° CGLAT), the bays changed their sign again and became negative (~−120 nT). Negative bays were recorded in Bork (BOX, ~54.5° CGLAT, Rus-

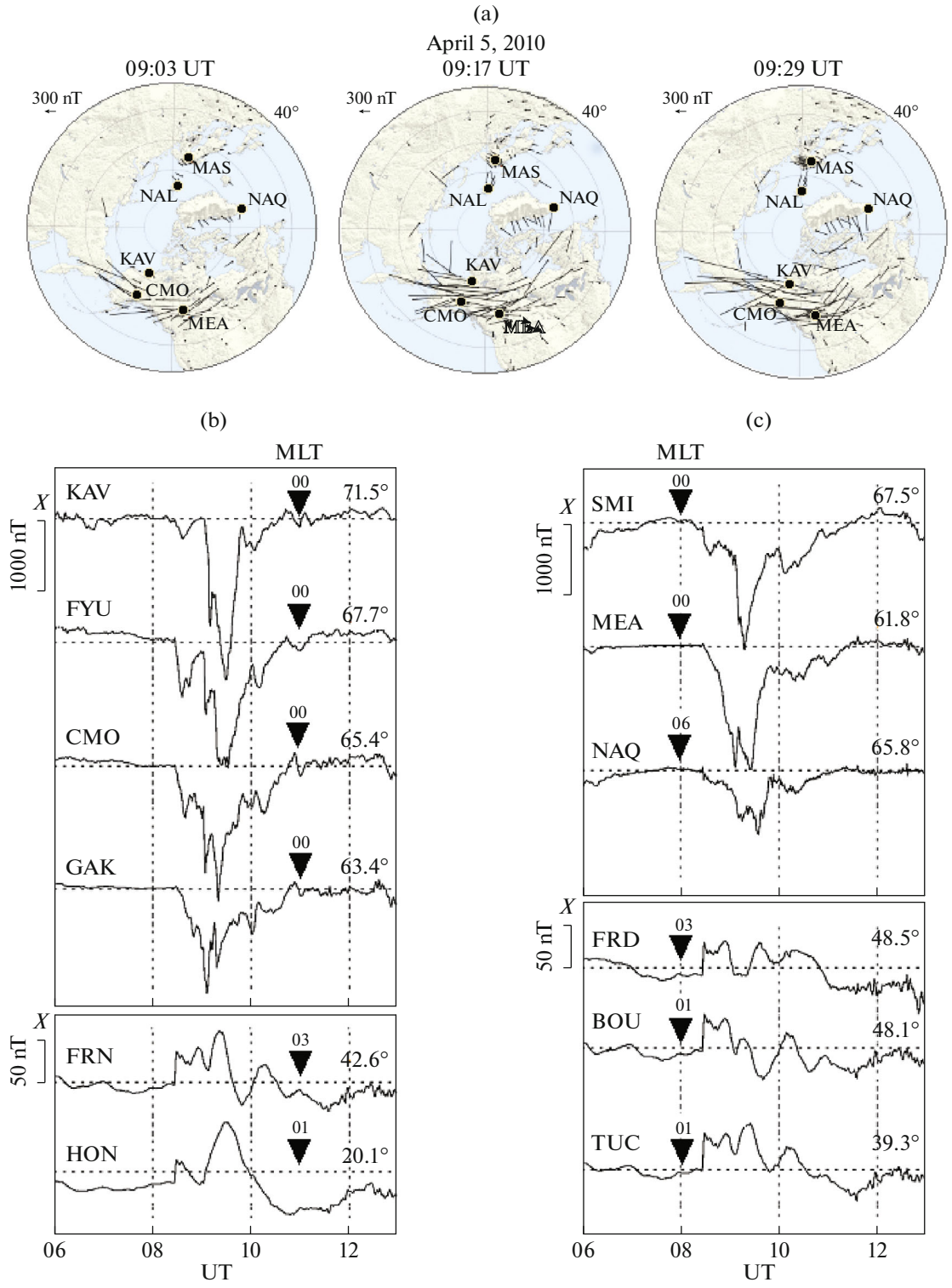

Fig. 2. Development of magnetic disturbances, according to SuperMAG data. The instantaneous maps (09:03, 09:17, and 09:29 UT) of magnetic disturbances with indicated ground-based stations: (a) Midnight (bottom), noon (top); *X* component of the magnetic field from 06:00 to 13:00 UT on April 5, 2010, for stations KAV, FYU, CMO, and GAK in Alaska (upper panel), and midlatitude stations FRN and HON (bottom panel). (b) The plot gives the names of the stations, the geomagnetic coordinates (CGLAT), and the MLTs (numbered arrows). (c) *X* component of the magnetic field for stations SMI, MEA, and NAQ in the auroral zone (upper panel) and midlatitude stations FRD, BOU, TUC (bottom panel).

sia), Kiev (KIV, ~46.6° CGLAT, Ukraine), and Panagyurishte (PAG, ~42.7° CGLAT, Bulgaria). Negative bays (~60 nT) also occurred in the vicinity of the equator at the TAM station (~8.9° CGLAT, Algeria). Thus, on the day side, we observed an unusual pattern in the latitudinal distribution of the magnetic disturbances that can be described as a layered cake.

To complete the global pattern of magnetic disturbances, we used data from magnetic observations by the AMPERE satellite mission. Figure 4 presents maps from a spherical harmonic analysis of the distribution of magnetic disturbance (on the left) and the field-aligned currents (on the right) calculated with these data for intervals close to 09:30 UT with indication of the positions of some ground-based stations. Downward currents are marked in blue; upward currents are shown in red. Magnetic data from the AMPERE satellite mission (the left panel in Fig. 4) illustrate the formation of an intense eastward electrojet over Eastern Siberia in the day–pre-midnight sector between downward and upward currents. Since there were no ground-based stations in this region, it is not seen on the SuperMAG map (Fig. 2). At the same time, the map in the left panel in Fig. 4, constructed using results from the spherical harmonic analysis of magnetic field recordings by low-apogee communication satellites of the AMPERE system, shows that the westward electrojet expanded from Alaska toward Scandinavia, through North America and Greenland (from the night side through the morning side to the day side). Both electrojets were detected over Scandinavia where the IMAGE meridian was found (Figs. 3 and 4), though at different latitudes. The westward electrojet was detected over Spitsbergen; the eastward one, at auroral latitudes. The westward current was detected again at subauroral and middle latitudes.

RESULTS AND DISCUSSION

Our analysis of the super substorm on April 5, 2010, showed that the westward electrojet extended considerably in longitude: from the evening sector (Alaska) to the morning sector (Greenland) and the day sector (Scandinavia). The most intense disturbances were recorded in the pre- and post-midnight sectors at auroral latitudes; weaker disturbances were observed at polar latitudes in the morning and day sectors. This confirms the results obtained in [9, 10] for other SSS events.

Figure 4 shows the development of the intense eastward electrojet in the early evening sector was a feature of the ionospheric currents during the SSS on April 5, 2010. The formation of such an eastward electrojet can be attributed to the unusual intensification of the partial ring current that was observed during this super substorm [16]. It is known that during magnetic storms associated with a bow shock and contraction of the magnetosphere, the ring current intensifies at around 12 MLT. But in this event, an additional increase in ring current was recorded at ~15 MLT. It was likely caused by interaction between charged par-

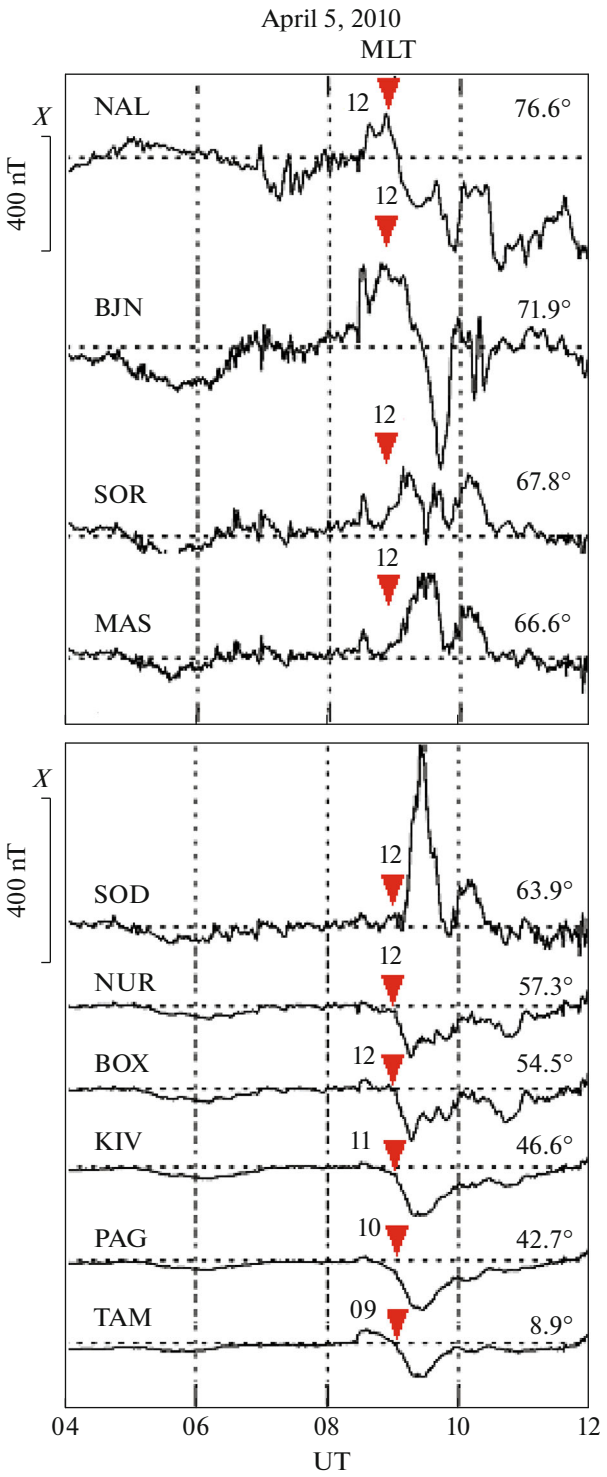

Fig. 3. *X* component of the magnetic field from 04:00 to 12:00 UT on April 5, 2010, for several stations of the IMAGE and SuperMAG networks. Upper panel: NAL, BJN, SOR, and MAS. Bottom panel: SOD, NUR, BOX, KIV, PAG, and TAM. The format is the same as in Fig. 2b.

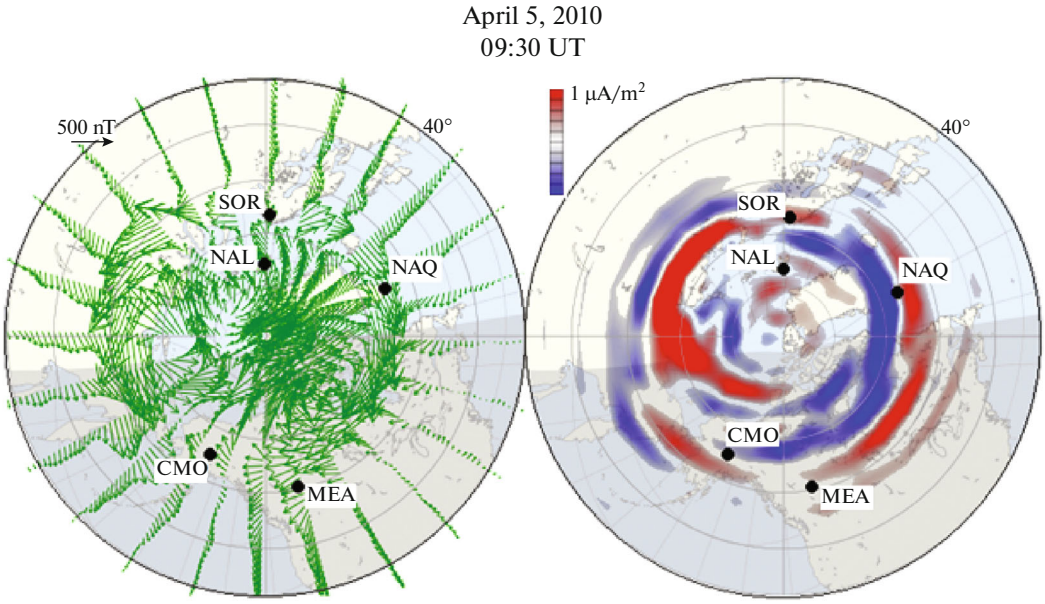

Fig. 4. Maps of magnetic disturbances and field-aligned currents, made with data from AMPERE satellite mission in corrected geomagnetic coordinates for the interval 09:26–09:36 UT. Location of ground-based stations are indicated. Left: Map from spherical harmonic analysis of magnetic disturbances. Right: Map of the distribution of field-aligned currents. The upward current is marked in red; the downward current, in blue. Midnight is at the bottom; noon. is at the top. The current density varies from −1 to +1 μA/m^2 on the color scale.

ticles in the inner magnetosphere and ULF waves resulting from a bow shock wave [16, 24, 25]. AMPERE data show this additional ring current was close to the ionosphere on the eastward electrojet (Fig. 4).

It is obvious that both electrojets (eastward and westward) developed on a global scale and tried to reach the day side, surrounding the polar cap from different sides. The alternating field-aligned currents associated with both electrojets thus occurred at different latitudes in the day sector, resulting in the formation of the complex layered pattern of field-aligned currents and their respective ground-based magnetic bays recorded on the IMAGE meridian.

CONCLUSIONS

The super substorm observed on April 5, 2010, was characterized by an unusual spatial pattern of auroral electrojet development. (1) There was a strong westward electrojet on a global scale in the evening and night sectors, from the evening side at auroral latitudes to the day side in the polar region. (2) A nontypical latitude effect of a layered cake in magnetic bays was recorded on the day side. It was attributed to the complex structure of field-aligned currents when the observer meridian was located near the ends of the westward and eastward electrojets. (3) Data from AMPERE satellite observations showed that in contrast to the typical scenario of the development of classical substorms, an intense eastward electrojet was registered during the considered super substorms in the pre-evening sector, confirming the hypothesis in [16] about the formation of an additional partial ring current close to the eastward electrojet during the SSS.

ACKNOWLEDGMENTS

The authors are grateful to the developers of such databases as OMNI (http://omniweb.gsfc.nasa.gov), SuperMAG (http://supermag.jhuapl.edu/), IMAGE (http://space.fmi.fi/image/), and AMPERE (http://ampere.jhuapl.edu) for allowing us to use them in this work.

FUNDING

The work of I.V. Despirak, N.G. Kleimenova, A.A. Lubchich, and P.V. Setsko was supported by the Russian Foundation for Basic Research, project no. 20-55-18003-Bulg_a. The work of L.I. Gromova was performed as part of a State Task for the Pushkov Institute of Terrestrial Magnetism, the Ionosphere, and Radio Wave Propagation. The work of V. Gineva was supported by the National Science Fund of Bulgaria, project no. КП-06-Русия/15.

REFERENCES

1. Tsurutani, B.T., Hajra, R., Echer, E., and Gjerloev, J.W., *Ann. Geophys.*, 2015, vol. 33, no. 5, p. 519.
2. Hajra, R., Tsurutani, B.T., Echer, E., et al., *J. Geophys. Res.*, 2016, vol. 121, no. 8, p. 7805.

3. Despirak, I.V., Lyubchich, A.A., and Kleimenova, N.G., *Geomagn. Aeron.*, 2019, vol. 59, no. 2, p. 170.
4. Despirak, I.V., Lubchich, A.A., and Kleimenova, N.G., *Proc. XLIII Ann. Seminar on Physics of Auroral Phenomena*, Apatity, 2020, p. 7.
5. Adhikari, B., Dahal, S., and Chapagain, N.P., *Earth Space Sci.*, 2017, vol. 4, no. 5, p. 257.
6. Adhikari, B., Baruwal, P., and Chapagain, N.P., *Earth Space Sci.*, 2017, vol. 4, no. 1, p. 2.
7. Tsurutani, B.T. and Hajra, R., *J. Space Weather Space Clim.*, 2021, vol. 11, 23.
8. Hajra, R. and Tsurutani, B.T., *Astrophys. J.*, 2018, vol. 858, no. 2.
9. Despirak, I.V., Kleimenova, N.G., Malysheva, L.M., et al., *Geomagn. Aeron.*, 2020, vol. 60, no. 3, p. 292.
10. Despirak, I.V., Lyubchich, A.A., Kleimenova, N.G., et al., *Bull. Russ. Acad. Sci.: Phys.*, 2021, vol. 85, no. 3, p. 246.
11. Kinrade, J., Mitchell, C.N., Yin, P., et al., *J. Geophys. Res.*, 2012, vol. 117, no. A5, A05304.
12. Lu, G., Hagan, M.E., Häusler, K., et al., *J. Geophys. Res.: Space Phys.*, 2014, vol. 119, no. 12, 10358.
13. Prikryl, P., Spogli, L., Jayachandran, P.T., et al., *Ann. Geophys.*, 2011, vol. 29, no. 12, p. 2287.
14. Kleimenova, N.G., Kozyreva, O.V., Malysheva, L.M., et al., *Geomagn. Aeron.*, 2013, vol. 53, no. 3, p. 313.
15. Nishimura, Y., Lyons, L.R., Gabrielse, C., et al., *J. Geophys. Res.: Space Phys.*, 2020, vol. 125, no. 4, e2019JA027654.
16. Zong, Q.-G., Yue, C., and Fu, S.-Y., *Space Sci. Rev.*, 2021, vol. 217, no. 2, p. 33.
17. McPherron, R.L. and Chu, X., *Space Sci. Rev.*, 2017, vol. 206, no. 1, nos. 1–4, p. 91.
18. Newell, P.T. and Gjerloev, J.W., *J. Geophys. Res.: Space Phys.*, 2011, vol. 116, no. A12, A12211.
19. Love, J.J., *Phys. Today*, 2008, vol. 61, no. 2, p. 31.
20. Viljanen, A. and Häkkinen L., *ESA Publications SP-1198*, 1997, p. 111.
21. Clausen, L.B., Baker, J.B.H., Ruohoniemi, J.M., et al., *J. Geophys. Res.: Space Phys.*, 2012, vol. 117, no. A6, A06233.
22. Yermolaev, Yu.I., Nikolaeva, N.S., Lodkina, I.G., and Yermolaev, M.Yu., *Cosmic Res.*, 2009, vol. 47, no. 2, p. 81.
23. Liu, Y., Luhmann, J.G., Bale, S.D., and Lin, R.P., *Astrophys. J.*, 2011, vol. 734, no. 2, p. 84.
24. Zong, Q.-G., Wang, Y.F., Zhang, H., et al., *J. Geophys. Res.: Space Phys.*, 2012, vol. 117, A11206.
25. Kozyreva, O.V., Pilipenko, V.A., Zakharov, V.I., and Engebretson, M.J., *GPS Solutions*, 2017, vol. 21, no. 3, p. 927.

Translated by L. Mukhortova